



Microstructural stability of long term aging treated Ti–22Al–26Nb–1Zr orthorhombic titanium aluminide

Tie-bang ZHANG, Gang HUANG, Rui HU, Jin-shan LI

State Key Laboratory of Solidification Processing, Northwestern Polytechnical University, Xi'an 710072, China

Received 28 September 2014; accepted 8 December 2014

Abstract: The microstructure development of lamellar structure of an orthorhombic Ti_2AlNb -based Ti–22Al–26Nb–1Zr alloy, including $B2$ decomposition and spheroidization of O phase, was investigated. The results show that the lamellar structure is fabricated by heating the samples in the single $B2$ phase field and cooling slowly in the furnace. Aging treatments are conducted in the ($O+B2$) phases field by air cooling. After aging at 700 °C for a short time within 100 h, there is no significant change of microstructures, whereas the coarsening of lamellae is observed in the long-term aged microstructure. Ti–22Al–26Nb–1Zr alloy exhibits microstructural instability including the severe dissolution of $B2$ lamella, discontinuous precipitation and spheroidization of O phase during the long term aging process at 700 °C up to 800 h. In addition, a pronounced formation of branch-shaped O phase lamella is observed for the alloy aged over 100 h.

Key words: orthorhombic titanium aluminide; microstructural evolution; aging treatment; spheroidization

1 Introduction

Ti_2AlNb -based alloys have been regarded as the most promising candidates for use in the aircraft engine materials in the past decades due to their low density and good high-temperature properties, and are verified to possess better mechanical properties over conventional α_2 -based alloys [1–3]. Especially the second generation orthorhombic alloys, such as Ti–22Al–25Nb and Ti–22Al–27Nb (mole fraction, %), with $O+B2$ lamellar microstructure preserve superior mechanical properties including high tensile strength, improved creep resistance as well as fracture toughness [4–8].

As a family of high-temperature used alloys, approximately 600 to 750 °C [9], the microstructural stability during aging in air environment is a key focus of Ti_2AlNb -based alloys. Whereas, the creep and mechanical properties of Ti_2AlNb -based alloys are significantly susceptible to microstructural evolution. It has been reported that $B2$ phase in Ti_2AlNb -based alloys is unstable and undergoes a decomposition around 700 °C [10]. The instabilities of $B2$ phase may pronouncedly degrade the creep properties and other high-temperature properties. YANG et al [11] have

observed an abnormal acceleration of creep rate and ascribed it to the formation of prismatic dislocations generated from O/BCC interfaces by the transformation of $B2$ phase to O phase above 700 °C. ROWE et al [12] have found that discontinuous precipitation could lead to high primary creep strains, and influenced the minimum creep rate in the long time creep process. Meanwhile, the work of LIN et al [13] indicates that Ti–22Al–25Nb exhibits a microstructural instability during the tensile deformation, characterized by coarsening, fragmentation, and spheroidization of the O phase. More recently, the O phase plates with a special type of arrangement, which account for the enhancement of microhardness, have been found by KHADZHIEVA et al [14] in the course of the $\beta \rightarrow O$ transformation during the aging process for 4 h. As multiphase alloys, the microstructural stability during high-temperature exposure always determines the practical applications of Ti_2AlNb -based intermetallic compounds. However, to date, only a limited number of reports focus on the microstructural evolution of Ti_2AlNb -based alloys in service temperature in contrast to γ -TiAl [15–18]. In order to give immediate guidance in the choice of prolonged aerospace application materials, it is necessary to understand the high-temperature microstructural stability of Ti_2AlNb -based

alloys at elevated temperatures.

Recently, a Zr-containing Ti_2AlZr phase has been found to be considerably stable, and the alloys with this phase possess high yield strength [19–21]. Additionally, the addition of Zr may also improve the creep resistance of Ti_2AlNb -based alloys [22]. Taking these advantages into consideration, the element of Zr is introduced to investigate its effect on the microstructural stability of Ti_2AlNb -based alloys to improve the high temperature properties to some extent. The present work mainly concerns to establish a fundamental understanding of the microstructural changes of a Zr-containing Ti_2AlNb -based alloy during the long-term aging treatment.

2 Experimental

The nominal composition of the test alloy was selected as Ti–22Al–26Nb–1Zr (mole fraction, %). The ingot was melted by vacuum consumable electrode melting from the commercial high-purity starting materials of Al shot, Ti sponge, Zr sponge and Ti–Nb binary alloy. The ingot was melted three times to ensure the chemical homogeneity. Then, the ingot was broken down in the $B2$ phase field, followed by an extra β forging plus a subtransus low temperature forging.

The forged Ti–22Al–26Nb–1Zr alloy was solution-treated at 1150 °C and then water-quenched. In order to obtain the lamellar microstructure, the cooling rate after the solution treatment was chosen as about 2.4 °C/min. Aging treatments were performed at 700 °C for various durations from 24 to 800 h after solution treatment. The microstructures of the specimens were characterized by optical microscopy, scanning electron microscopy (SEM) and transmission electron microscopy (TEM). The phase compositions of alloys were examined by X-ray diffraction, with the continuous scanning mode with 0.03° interval and 1.0 s counting time. The diffraction data were collected at room temperature on a DX–2700 diffractometer using Cu K_α radiation. The voltage and anode current were 40 kV and 30 mA, respectively. The thin foils for transmission electron microscopy were prepared by twin jet polishing in a solution of methanol, butanol and perchloric acid at –20 to –30 °C. Transmission electron microscopy (TEM) was performed using an FEI Tecnai G2 F30 TEM equipped with an energy-dispersive X-ray (EDX) detector and operated at 300 kV.

3 Results

3.1 Microstructure of solution-treated alloy

The microstructures of solution-treated Ti–22Al–26Nb–1Zr alloy are shown in Fig. 1. Figure 1(a) shows an optical image of lamellar microstructure in the prior

$B2$ phase. The typical lamellar colony (in section *A*) and Widmanstätten lath (in section *B*) are apparently observed, and equiaxed constituents are avoided. In Fig. 1(b), the dark section can be ascribed to α_2 phase, the bright and gray sections are $B2$ and O phases, respectively, which is consistent with the observation in Ref. [23]. The α_2 phase locates inside the grain exists as long aligned lath caused by supertransus processing and irregular shape block [24]. However, the formation of irregular shape blocks has not been well determined yet. Figure 2 shows the X-ray diffraction pattern of the as-soluted sample, which confirms the presence of α_2 , BCC and O phases, and the ordered $B2$ phase is

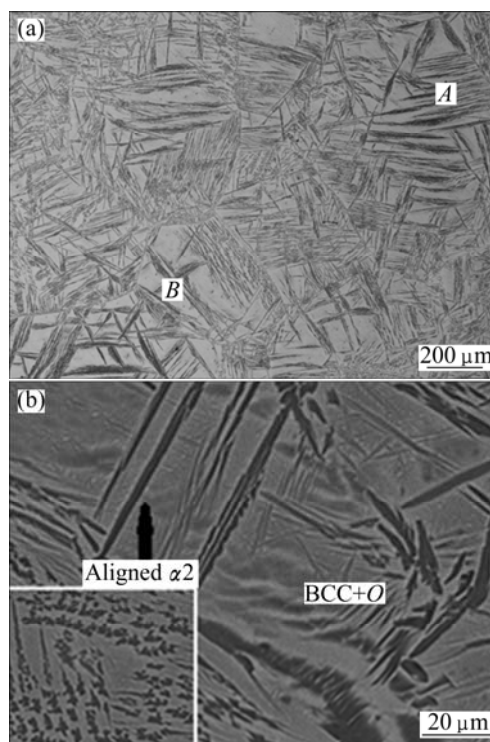


Fig. 1 Optical (a) and back scattered SEM (b) images of Ti–22Al–26Nb–1Zr alloy after heating in the $B2$ phase field for 1 h followed by furnace cooling

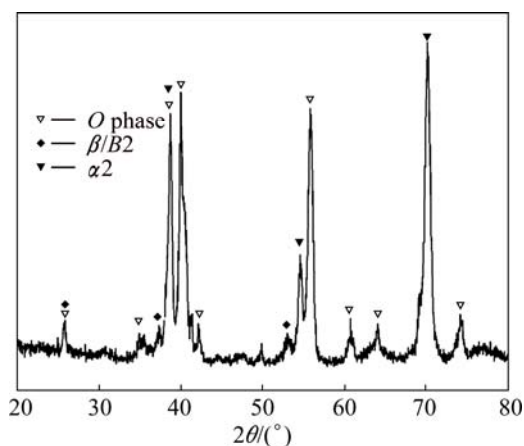


Fig. 2 X-ray diffraction pattern of as-soluted Ti–22Al–26Nb–1Zr alloy

identified by its (100) peak [24]. No Bragg peaks of Zr-containing precipitate are observed in the XRD spectra.

3.2 Microstructural evolution of aged alloys

3.2.1 Dissolution of $B2$ lamella in aging process

The micrographs in Figs. 3(a) and (b) reveal the microstructures of the alloys aged for 24 and 100 h, respectively, which show no significant difference from the starting condition (Fig. 1(b)), and only $B2$ lamella can be observed in the alloy, as indicated by the arrow in Fig. 3(a). There is almost no $B2$ lamellae decomposing into O and β phases during the aging process for 24 and 100 h. After 200 h, $B2$ lamellae begin to decompose in the bulk, as indicated by the arrow in Fig. 3(c). It is necessary to note that some coarse O blocks precipitate discontinuously at the $O/B2$ phase interfaces. However, this discontinuous precipitation is inconsistent with the report in Ref. [25] to some extent, where the typical discontinuous precipitation initiated only at the grain boundaries, as shown in Fig. 3(a), rather than at the $O/B2$ phase interfaces. It is generally believed that only the grain boundaries favor the process of discontinuous precipitation, while the precipitate/matrix boundaries, especially the matrix and the eutectoid phases interfaces, may also act as the same role as the grain boundaries [26]. Moreover, the precipitates are observed with alternating the platelets morphologies. It has been reported that the addition of Zr could influence the distribution and morphology of ω particles in the γ -TiAl alloy [27], probably the precipitation sites and the

morphology of O phase are inevitably affected by the addition of Zr.

The microstructures of samples aged for 800 and 480 h are shown in Fig. 3(d) and Fig. 4, respectively. The occurrence of dissolution of $B2$ lamella in the long time aged alloys is not evident, which is in agreement with the observations reported by BOEHLERT et al [25] that the phase transformation occurred rapidly in the bulk at 650 °C. It is reasonable to say that this transformation will take less time at 700 °C. This is also evidenced by the X-ray diffraction spectra in Fig. 5, the intensity of peaks of $B2$ phase keep almost stable after aging treatment for 100 h. However, the super-lattice peaks of $B2$ phase still remain in each specimen aged for various time, giving the evidence that $B2$ phase is retained even after aging for 800 h. This is probably due to the fact that the decomposition of $B2$ phase is incomplete, or the re-precipitation of $B2$ phase throughout the O phase occurs [28,29]. Apparent branches of O phase are observed in the alloy aged for 800 h, as indicated by arrows in Fig. 3(d). The TEM micrograph of alloy aged for 200 h, as indicated by the arrow in Fig. 6, also gives the evidences about the discontinuous precipitation of O blocks. This phenomenon cannot be observed in the microstructure images of the alloys aged at 700 °C for 24 and 100 h, as shown in Figs. 3(a) and (b), respectively.

3.2.2 Spheroidization and formation of branch-shaped O phase lamella

Compared with the microstructures of the short-time aged specimens, O phase lamellae undergo considerable coarsening after 480 h. With the dissolution

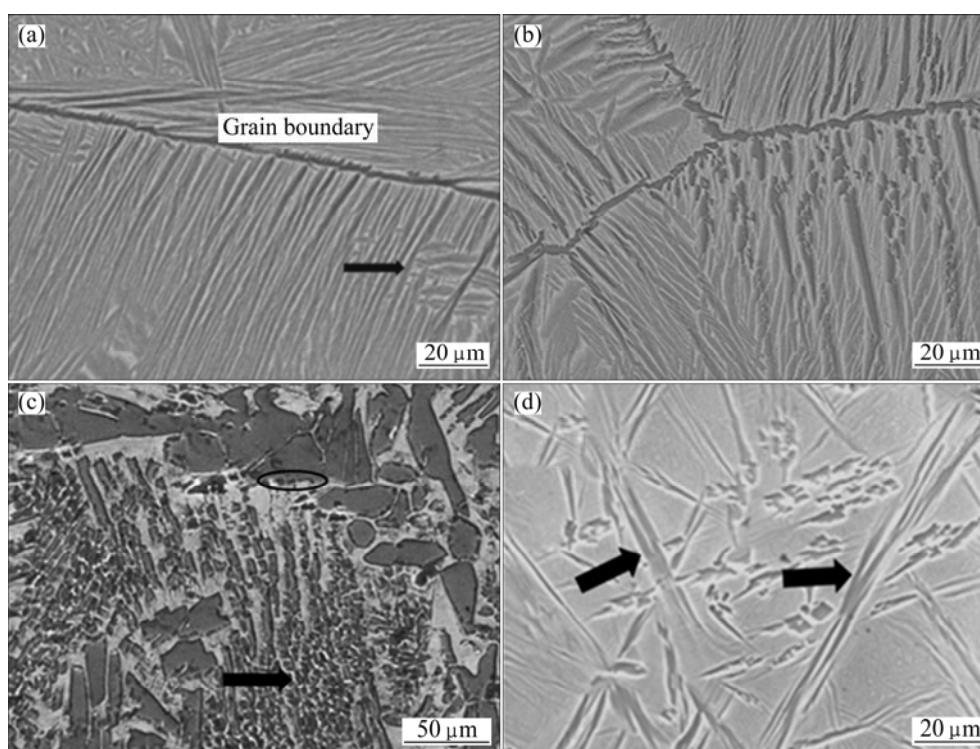


Fig. 3 Back scattered SEM images of Ti-22Al-26Nb-1Zr aged at 700 °C for different time: (a) 24 h; (b) 100 h; (c) 200 h; (d) 800 h

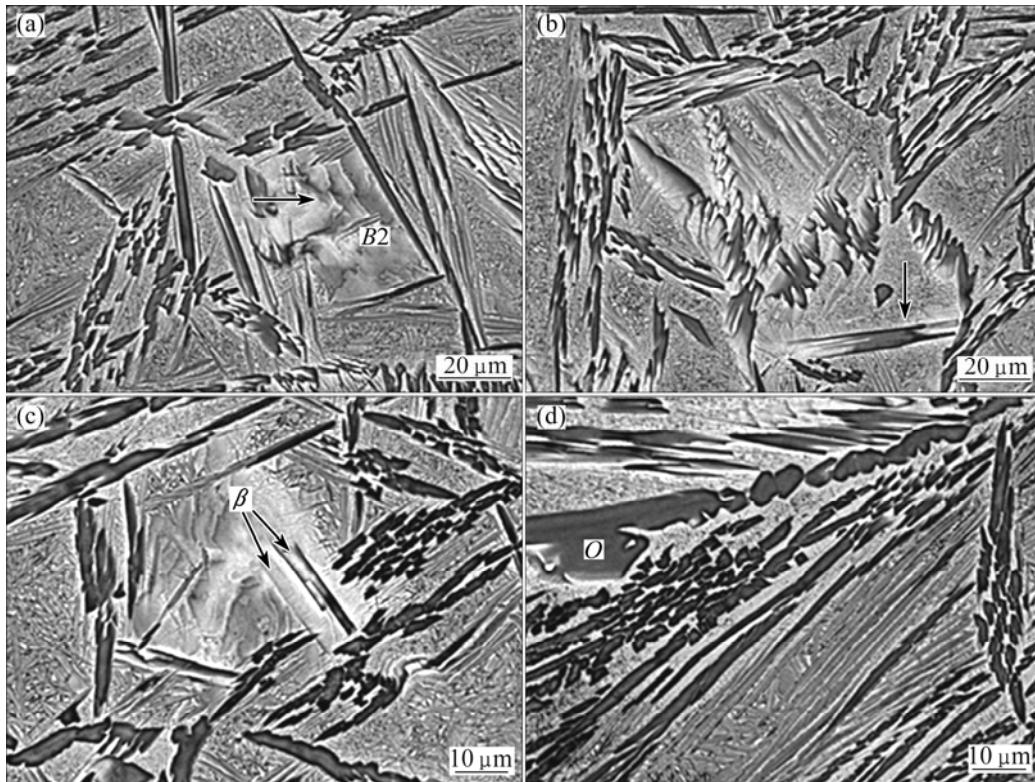


Fig. 4 Back scattered SEM images of Ti-22Al-26Nb-1Zr alloy aged at 700 °C for 480 h taken in different zones: (a) Stacked coarse sheet; (b) Bifurcation of *O* lamella; (c) Cylinderization of *O* lamella; (d) Spheroidization of *O* lamella

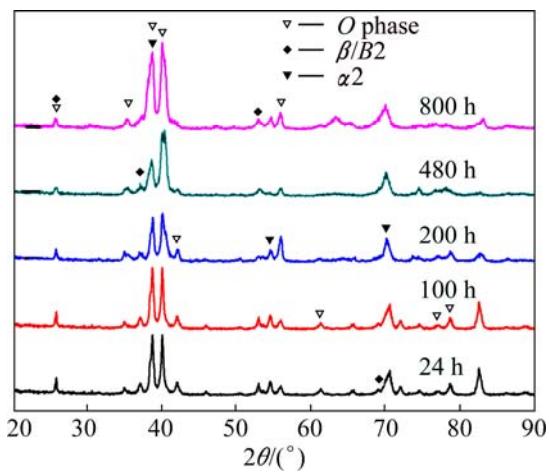


Fig. 5 XRD spectra of specimens aged at 700 °C for 24, 100, 200, 480 and 800 h

of *B2* phase, the increased *O* phase blocks or plates are formed at the *O/B2* interfaces, as observed in Ref. [25]. The separate *O* blocks inside the *B2* regions are finally connected to each other by means of constant discontinuous precipitation of *O* phase, the primary *O* lamellae coarsened by the migration of *O/BCC* interfaces towards the transformed *B2* lamellae. The fine *O* phase lamellae prior to aging treatment transform to coarse rods after 200 h. In addition, the size and morphology of α_2 phase undergo fundamental changes, equiaxed α_2

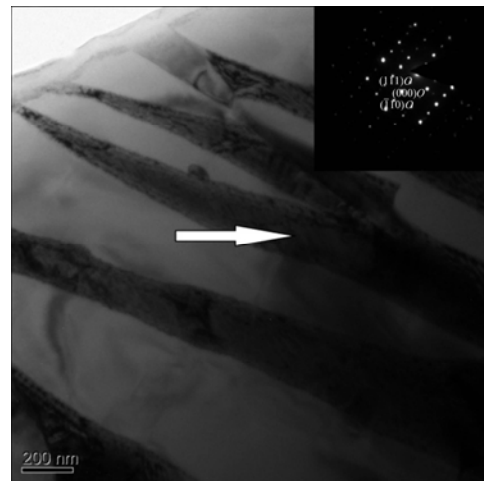


Fig. 6 Bright field image of branch-shaped *O* lamellae in samples aged at 700 °C for 200 h

particles transform to coarse lenticular fashion, and aligned α_2 phase becomes much slender and coarser than that in the un-aged alloy.

In Fig. 4, four types of microstructural changes of sample aged for 480 h are observed. In Fig. 4(a), the (*O+B2*) lamellae have disappeared in some colonies, which are replaced by the stacked coarse layers, as the arrow indicates. The work of BOEHLERT [28] has indicated that the layer is a BCC phase with no

precipitated lath or needle in the layer. The branches indicated by the arrow in Fig. 4(b) can be only seen in TEM images of samples aging less than 480 h. However, the samples aged separately for 480 and 800 h show the same phenomenon, as indicated in the SEM images. The lamellae or laths dissolve into large packets (arrowed in Fig. 4(c)), which can be mainly attributed to β phase due to its low Al and high Nb contents, as have been observed by BOEHLERT [28]. With the progress of coarsening and decomposition, several coarse O lamellae break up into segments, each segment begins to be spheroidized individually, as shown in Fig. 4(d).

4 Discussion

The principal evolution of microstructural changes during the aging process at service temperature can be described as follows. Firstly, O phase blocks discontinuous precipitate and part of them are spheroidized. Then, the stacked coarse layers form for the dissolution of Widmanstätten laths and lamellae in some colony packets or at the grain boundaries. Finally, branch-shaped lamellae will be generated in the long time aged sample. The $B2$ phase transformation to an orthorhombic phase during aging can be attributed to higher heat of formation of the $B2$ phase than that of Zr-containing phase and orthorhombic structure [19]. The results in this work indicate that the addition of Zr probably favors the phase transformation from $B2$ phase to an orthorhombic phase. Similar results have been observed in γ -TiAl compounds that Zr tends to form fault-like features and acts as precursors for the formation of γ lamellae. As a result, the lamellar decomposition from α to $\alpha_2+\gamma$ in Zr-containing γ -TiAl will be accelerated [30].

It is known that the discontinuous precipitation is a grain boundary-diffusion controlled process [25], a high volume fraction of α_2 phase retained along the grain boundaries (as shown in Fig. 1(b)), which probably hinders the original diffusion route to some extent and thus favors the phase boundary diffusion. In addition, the misfit dislocations formed preferentially at the O /BCC interfaces may also facilitate the precipitation at the phase boundaries [28]. As the circle indicated in Fig. 3(c), “double-seam” morphology is observed. This phenomenon favors the initiation of discontinuous precipitation which is consistent with the precipitate-assisted mechanism where the initial precipitates are capable of acting immediately to displace the grain boundaries [31], as can be observed in the darkest zones shown in the precipitated O blocks in Fig. 3(c). Therefore, the discontinuous precipitation is preferentially located at the phase interfaces rather than

the grain boundaries. Upon slow cooling after solution treatment, the degree of supersaturation of $B2$ phase lessened [28]. Compared with the water quenched microstructure in the aging process, the precipitated O phase is capable of keeping stable by reducing the interfacial free energy and the corresponding total free energy, namely, they can exist stably as blocks. This is the reason why the morphology of precipitated O phase varies, as indicated in Ref. [25].

The formation of branch-shaped lamella is a direct result of the discontinuous precipitation of O phase, the similar morphology is also found in Ref. [32]. The fact that the quantity of branches increases with increasing the aging time probably results from the discontinuous precipitation region interacting with each other. It depends on where the repeated nucleation during discontinuous precipitation begins [33]. The coarsening of the lamellar microstructure occurs behind the migrating of BCC grain boundary [34].

The discontinuous precipitation becomes less pronounced and tends to be followed by classical coarsening during the aging progress [34]. It is often observed that the Widmanstätten laths and lamellae in some colony packets or near the grain boundaries coarsen severely to large layers, while discontinuous precipitation is responsible for the formation of coarse layers [25]. The atoms between the adjacent O phase constantly migrate to other zones, then the two adjacent spheroidized O lamellae gradually approach to each other and continue to coarsen separately without growing to the whole layer. Then, a large number of atoms accumulate at the grain boundary. As a result, one layer begins to grow on the surface of another until this process is completed.

5 Conclusions

1) The severe microstructural degeneration of Ti-22Al-26Nb-1Zr alloy can be observed during the long-term aging treatment. Ti-22Al-26Nb-1Zr alloy exhibits microstructural instability due to the thermodynamical equilibrium of lamellar microstructures.

2) The microstructural instability of Ti-22Al-26Nb-1Zr alloy includes the dissolution of $B2$ lamellae, discontinuous precipitation of O phase, spheroidization of O phase and formation of coarse layers during long-term aging process at 700 °C up to 800 h.

3) A pronounced formation of branch-shaped O phase lamella is observed for the alloy aged over 100 h. The degeneration of the lamellar microstructure can be ascribed to the phase decomposition and discontinuous precipitation.

References

- [1] BANERJEE D, GOGIA A K, NANDI T K, JOSHI V A. A new ordered orthorhombic phase in a Ti₃Al–Nb alloy [J]. Acta Metallurgica, 1988, 36(4): 871–882.
- [2] SONG Hui, WANG Zhong-jin, HE Xiao-dong. Improving in plasticity of orthorhombic Ti₂AlNb-based alloys sheet by high density electropulsing [J]. Transactions of Nonferrous Metals Society of China, 2013, 23(1): 32–37.
- [3] WANG Y X, ZHANG K F, LI B Y. Microstructure and high temperature tensile properties of Ti₂₂Al₂₅Nb alloy prepared by reactive sintering with element powders [J]. Materials Science and Engineering A, 2014, 608: 229–233.
- [4] XUE C, ZENG W, WANG W, LIANG X, ZHANG J. Quantitative analysis on microstructure evolution and tensile property for the isothermally forged Ti₂AlNb based alloy during heat treatment [J]. Materials Science and Engineering A, 2013, 573(0): 183–189.
- [5] EMURA S, ARAOKA A, HAGIWARA M. B2 grain size refinement and its effect on room temperature tensile properties of a Ti–22Al–27Nb orthorhombic intermetallic alloy [J]. Scripta Materialia, 2003, 48(5): 629–634.
- [6] NICOLAOU P, SEMIATIN S. High-temperature deformation and failure of an orthorhombic titanium aluminide sheet material [J]. Metallurgical and Materials Transactions A, 1996, 27(11): 3675–3681.
- [7] MAO Y, LI S Q, ZHANG J W, PENG J H, ZOU D X, ZHONG Z Y. Microstructure and tensile properties of orthorhombic Ti–Al–Nb–Ta alloys [J]. Intermetallics, 2000, 8(5–6): 659–662.
- [8] WU Hong-yan, ZHANG Ping-ze, CHEN Wei, WANG Ling, ZHAO Hao-feng, XU Zhong. High-temperature tribological behaviors of Ti₂AlNb-based alloys by plasma surface duplex treatment [J]. Transactions of Nonferrous Metals Society of China, 2009, 19(5): 1121–1125.
- [9] SEMIATIN S L, SMITH P R. Microstructural evolution during rolling of Ti–22Al–23Nb sheet [J]. Materials Science and Engineering A, 1995, 202(1–2): 26–35.
- [10] LI D, BOEHLERT C. Processing effects on the grain-boundary character distribution of the orthorhombic phase in Ti–Al–Nb alloys [J]. Metallurgical and Materials Transactions A, 2005, 36(10): 2569–2584.
- [11] YANG S J, NAM S W, HAGIWARA M. Abnormal acceleration of creep deformation rate above 700 °C in the orthorhombic based Ti–22Al–27Nb alloy [J]. Journal of Alloys and Compounds, 2004, 368(1–2): 197–210.
- [12] ROWE R G, GIGLIOTTI M F X, MARQUARDT B J. Creep and discontinuous precipitation in a Ti₃Al–Nb alloy at 923 K [J]. Scripta Metallurgica et Materialia, 1990, 24(7): 1209–1214.
- [13] LIN P, HE Z B, YUAN S J, SHEN J, HUANG Y J, LIANG X B. Instability of the O-phase in Ti–22Al–25Nb alloy during elevated-temperature deformation [J]. Journal of Alloys and Compounds, 2013, 578: 96–102.
- [14] KHADZHIEVA O G, ILLARIONOV A G, POPOV A A. Effect of aging on structure and properties of quenched alloy based on orthorhombic titanium aluminide Ti₂AlNb [J]. Physics of Metals and Metallography, 2014, 115(1): 12–20.
- [15] RAMANUJAN R V, MAZIASZ P J, LIU C T. The thermal stability of the microstructure of γ -based titanium aluminides [J]. Acta Materialia, 1996, 44(7): 2611–2642.
- [16] MAZIASZ P J, RAMANUJAN R V, LIU C T, WRIGHT J L. Effects of B and W alloying additions on the formation and stability of lamellar structures in two-phase [gamma]-TiAl [J]. Intermetallics, 1997, 5(2): 83–95.
- [17] HU D, GODFREY A B, LORETTO M H. Thermal stability of a fully lamellar Ti–48Al–2Cr–2Nb–1B alloy [J]. Intermetallics, 1998, 6(5): 413–417.
- [18] HUANG Z W, CONG T. Microstructural instability and embrittlement behaviour of an Al-lean, high-Nb gamma-TiAl-based alloy subjected to a long-term thermal exposure in air [J]. Intermetallics, 2010, 18(1): 161–172.
- [19] PREMKUMAR M, PRASAD K S, SINGH A K. Structure and stability of the B2 phase in Ti–25Al–25Zr alloy [J]. Intermetallics, 2009, 17(3): 142–145.
- [20] PREMKUMAR M, SINGH A K. Deformation behavior of an ordered B2 phase in Ti–25Al–25Zr alloy [J]. Intermetallics, 2010, 18(1): 199–201.
- [21] PREMKUMAR M, SINGH A K. Strength anomaly of the B2 phase in Ti–25Al–25Zr alloy [J]. Intermetallics, 2011, 19(7): 1085–1088.
- [22] GERMAN L, BANERJEE D, GUEDOU J Y, STRUDEL J L. Effect of composition on the mechanical properties of newly developed Ti₂AlNb-based titanium aluminide [J]. Intermetallics, 2005, 13(9): 920–924.
- [23] COWEN C J, BOEHLERT C J. Microstructure, creep, and tensile behavior of a Ti–21Al–29Nb(at.%) orthorhombic+B2 alloy [J]. Intermetallics, 2006, 14(4): 412–422.
- [24] RHODES C G. Orthorhombic titanium matrix composites [C]//SMITH P R. Materials and Manufacturing Directory. Dayton, OH: Air Force Research Laboratory, 1997: 83–100.
- [25] BOEHLERT C J, MAJUMDAR B S, SEETHARAMAN V, MIRACLE D B. Part I. The microstructural evolution in Ti–Al–Nb O+BCC orthorhombic alloys [J]. Metallurgical and Materials Transactions A, 1999, 30(9): 2305–2323.
- [26] BOUMERZOUZ Z, HAMANA D. Different sites of discontinuous precipitation and mechanisms of dissolution in Cu–9 wt.% Sb alloy [J]. Materials Chemistry and Physics, 2001, 69(1–3): 10–18.
- [27] JIANG H, HU D, WU X. Thermal stability of the omega phase in Zr-containing TiAl alloys [J]. Journal of Alloys and Compounds, 2009, 475(1–2): 134–138.
- [28] BOEHLERT C. The phase evolution and microstructural stability of an orthorhombic Ti–23Al–27Nb alloy [J]. Journal of Phase Equilibria, 1999, 20(2): 101–108.
- [29] MURALEEDHARAN K, NANDY T K, BANERJEE D, LELE S. Transformations in a Ti–24Al–15Nb alloy: Part II. A composition invariant $\beta_0 \rightarrow O$ transformation [J]. Metallurgical Transactions A, 1992, 23(2): 417–431.
- [30] ZHANG L C, CHENG T T, AINDOW M. Nucleation of the lamellar decomposition in a Ti–44Al–4Nb–4Zr alloy [J]. Acta Materialia, 2004, 52(1): 191–197.
- [31] FINDIK F. Discontinuous (cellular) precipitation [J]. Journal of Materials Science Letters, 1998, 17(1): 79–83.
- [32] YANG S J, NAM S W, HAGIWARA M. Investigation of creep deformation mechanisms and environmental effects on creep resistance in a Ti₂AlNb based intermetallic alloy [J]. Intermetallics, 2004, 12(3): 261–274.
- [33] MITAO S, BENDERSKY L A. Morphology and growth kinetics of discontinuous coarsening in fully lamellar Ti–44Al (at.%) alloy [J]. Acta Materialia, 1997, 45(11): 4475–4489.
- [34] DENQUIN A, NAKA S. Phase transformation mechanisms involved in two-phase TiAl-based alloys—I. Lamellar structure formation [J]. Acta Materialia, 1996, 44(1): 343–352.

Ti-22Al-26Nb-1Zr 合金在 长期时效过程中的组织稳定性

张铁邦, 黄刚, 胡锐, 李金山

西北工业大学 凝固技术国家重点实验室, 西安 710072

摘要: 研究正交结构 Ti-22Al-26Nb-1Zr 合金片层组织在长期时效过程中 $B2$ 相的分解、 O 相板条的球化等显微组织演变规律。结果表明: 合金加热到 $B2$ 单相区炉冷后可以获得板条组织, 在 $(O+B2)$ 相区 $700\text{ }^{\circ}\text{C}$ 时效 100 h 以内显微组织无明显变化。但在长时时效过程中板条组织发生明显粗化。在 $700\text{ }^{\circ}\text{C}$ 长期时效 800 h 时, $B2$ 相极不稳定, 会在时效初期短时间内迅速发生分解。随着时效时间的延长, 块状和少量板条状 O 相在晶界和 O/BCC 相界面析出并以球状形式长大。此外, 在时效时间超过 100 h 后, 会有明显的树枝状 O 相板条组织形成。

关键词: O 相 TiAl 合金; 组织演化; 时效处理; 球化

(Edited by Mu-lan QIN)